ORGANOMETALLICS

pubs.acs.org/Organometallics Article

Ligand Effects on Decarbonylation of Palladium-Acyl Complexes

Tedd C. Wiessner, Samuel Asiedu Fosu, Riffat Parveen, Nigam P. Rath, Bess Vlaisavljevich,* and William B. Tolman*

Cite This: https://dx.doi.org/10.1021/acs.organomet.0c00584 Read Online

ACCESS | Metrics & More | Article Recommendations | Supporting Information

ABSTRACT: The influences of perturbations of supporting phosphine ligands on the dehydrative decarbonylation of $(L_n)Pd^{II}(Cl)$-hydrocinnamoyl complexes (L = P^tBu_3, n = 1; L = PPh_3, n = 2; L = dppe, n = 1) to yield styrene were studied through combined experiment and theory. Abstraction of chloride from the complexes by silver and zinc salts, as well as sodium tetrakis[3,5-bis(trifluoromethyl)phenyl]borate, enhanced the efficiency of styrene formation, according to the following trend in L: P^tBu_3 > dppe > PPh_3. DFT calculations corroborated the experimental findings and provided insights into the ligand influences on reaction step barriers and transition state structures. Key findings include the following: a stable intermediate forms after chloride abstraction, from which β-hydride elimination is most affected by ligand choice, the low coordination number for the P^tBu_3 case lowers reaction barriers for all steps, and the *trans* disposition of two ligands for L = PPh_3 contributes to the low efficiency for styrene production in that case.

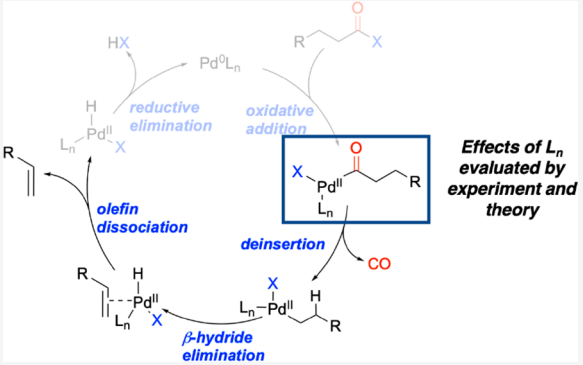

INTRODUCTION

Linear α-olefins (LAOs) are important commodity chemicals typically derived from petroleum feedstocks through ethylene oligomerization, generated in even-numbered chain lengths following a Flory–Schulz distribution.[1] An attractive, "green" alternative is the dehydrative decarbonylation of biorenewable carboxylic acids, particularly fatty acid derivatives.[2,3] Catalytic conversions of carboxylic acids to olefins usually requires activation of the acid, as illustrated by examples using *p*-nitrophenyl esters,[4] anhydrides,[5] or acyl halides.[6] Catalysts comprising complexes of Rh,[5d,7] Ru,[8] Ir,[9] Fe,[10] Ni,[4b] and, most commonly, Pd[3,5,11] have been developed. Photoredox methods undergo a different, single-electron pathway for the synthesis of olefins directly from the carboxylic acid.[12]

The mechanism for the catalytic dehydrative decarbonylation of carboxylic acid derivatives is generally thought to proceed as shown in Scheme 1.[13] According to this pathway, a low-valent metal, M, undergoes oxidative addition into the acyl C–X bond of the carboxylic acid derivative to form intermediate **B**, which subsequently undergoes deinsertion to form metal–alkyl complex **C**. The olefin complex **D** forms via β-hydride elimination. It ejects the product olefin and reductively eliminates HX to regenerate the active catalyst. Previous computational studies[13] indicated that oxidative addition is not rate-determining for appropriately activating X groups and that the greatest barriers arise along the deinsertion and β-hydride elimination path (**B** → **D**). While this mechanism is useful as a general framework, differences among the supporting ligands (L), metal ion (M), and activating group (X) likely affect the kinetics, thermodynamics, and structures of the intermediates, with the dissection of these influences being important for future catalyst design.

Scheme 1. Plausible Catalytic Cycle for the Decarbonylative Dehydrogenation of Fatty Acid Derivatives[a]

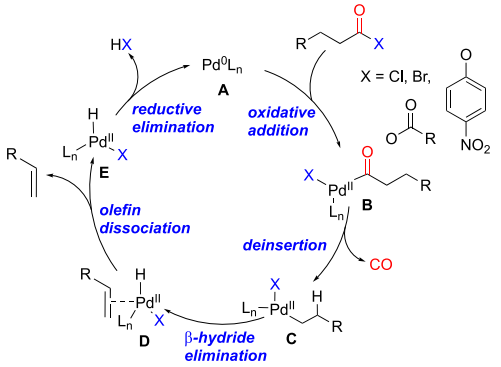

[a]M denotes a metal, L_n denotes the ligand with n being the number of ligands.

Received: September 1, 2020

https://dx.doi.org/10.1021/acs.organomet.0c00584
Organometallics XXXX, XXX, XXX–XXX

With the overarching aim of understanding catalyst structural effects on catalytic activity, we chose to focus on the specific effects of varying the supporting ligands in Pd complexes on the deinsertion and β-hydride elimination steps. Toward this end, we chose to examine the reactivity of Pd-acyl complexes of type **B**, derived specifically from hydrocinnamoyl chloride, because styrene would be the only possible olefin product (i.e., chain walking is avoided). We further focused on complexes bound to ligands P^tBu_3, PPh_3, and dppe (1,2-bis(diphenylphosphino)ethane)) in order to evaluate steric effects on the coordination environment and reactivity. The bulky P^tBu_3 has a large cone angle (θ) of 182° and a buried volume ($V_{\%bur}$) of 38.1% (measured by R_3P-AuCl), which has been reported to induce a three-coordinate geometry in Pd-acyl species.[14] On the other hand, PPh_3 is significantly smaller (θ = 145°, $V_{\%bur}$ = 29.9% on AuCl), forming four-coordinate *trans*-phosphine complexes on Pd.[15] The ligand dppe (θ = 218.6°, $V_{\%bur}$ = 51.4% on $PdCl_2$ or 29.2% on $(AuCl)_2$) is similar in size to two PPh_3 ligands but is constrained to adopt a *cis*-phosphine geometry.[16] With the aim of evaluating how these differences affected the deinsertion and β-hydride elimination steps, we targeted Pd-hydrocinnamoyl complexes for synthesis and reactivity studies, with experimental studies informed by theory. The findings we report herein reveal clear influences of the phosphine structure on the mechanism of deinsertion and β-hydride elimination, with possible implications for future catalyst design.

RESULTS AND DISCUSSION

Experiment. The Pd-hydrocinnamoyl complexes **1**−**3** were prepared as shown in Scheme 2. Compound **1** was identified

Scheme 2. Syntheses of 1−3

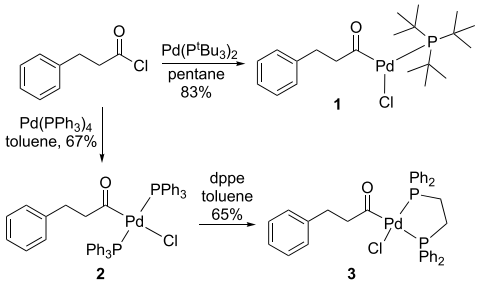

by a comparison of its ^1H and $^{13}C\{^1H\}$ NMR spectra and X-ray crystal structure with data previously reported;[14] **2** and **3** were characterized by ^1H, $^{13}C\{^1H\}$, and ^{31}P NMR spectroscopy and X-ray crystallography (Figure 1). While **1** adopts a slightly distorted T-shaped geometry with the phosphine ligand *trans* to chloride, **2** and **3** are square planar with *trans* and *cis* phosphine ligands, respectively. ^{31}P NMR spectra are consistent with retention of the solid-state coordination environments in solution, as **2** exhibits only one peak at 19.6 ppm for two equivalent phosphine ligands and **3** shows two coupled doublets, indicating inequivalent P atoms in a *cis* geometry (37.7 and 20.5 ppm, J = 44 Hz). Comparison of the hydrocinnamoyl methylene peaks in ^1H NMR spectra for the three complexes shows a trend in δ of **2** (1.51/2.19 ppm) < **3** (2.43/2.76 ppm) < **1** (2.89/3.54 ppm) that we attribute to *trans* influences that may be important in the reactivity of the complexes (*vide infra*). Thus, a *trans* chloride in **2** induces the most upfield chemical shift, a *trans*-$PRPh_2$ (R = methylene)

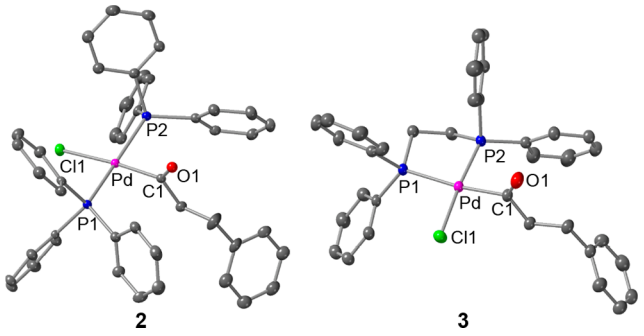

Figure 1. Representations of the X-ray crystal structures of **2** and **3** showing all non-hydrogen atoms as 50% thermal ellipsoids. Selected bond distances (Å): **2**, Pd−C(1) 1.983(2), Pd−P(1) 2.3486(5), Pd−P(2) 2.3393(5), Pd−Cl(1) 2.4291(5), O(1)−C(1) 1.191(2); **3**, Pd−C(1) 2.033(2), Pd−P(1) 2.3956(5), Pd−P(2) 2.2331(5), Pd−Cl(1) 2.3693(5), O(1)−C(1) 1.201(3).

moiety in **3** has an intermediate effect, and the absence of a *trans* ligand in **1** results in the most downfield peaks.

The complexes **1**−**3** are stable at room temperature, even in air for several days. In initial studies of their reactivity, solutions of the complexes in CH_3CN or THF were heated (T = 40−65 °C) in attempts to induce decarbonylation and identify intermediates. In every case, the starting material decayed gradually (12−24 h) and some styrene was observed (most effectively by **1**, 40 °C for 12 h, Figure S1). However, product mixtures formed, and the components were challenging to identify (^1H NMR spectroscopy, Supporting Information). Hypothesizing that initial decarbonylation would be facilitated by coordinative unsaturation at the metal center (supported by density functional theory (DFT) results described below), we sought to remove the chloride ligands in the complexes by treating them with silver and zinc salts, as well as $NaBAr^F$ (sodium tetrakis[3,5-bis(trifluoromethyl)-phenyl]borate; Table 1).

Table 1. Conversions of Pd-Acyl Complexes to Styrene[a]

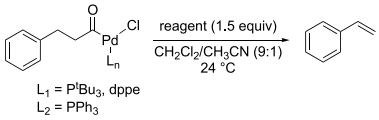

	conversion (%)		
additive	1	2	3
$AgBF_4$	>99	<5[b]	20[c]
$NaBAr^F$	>99	<5[b]	15[c]
$ZnCl_2$	>99	7[b]	19
$Zn(OAc)_2$	77	<3	25
ZnO	15	7	0
D^IPT	64	3	0

[a]Determined by in situ ^1H NMR spectroscopy. D^IPT = 1,3-diisopropyl-2-thiourea. Reactions of **1** were performed in acetonitrile-d_3. [b]Cationic complex also formed. [c]3-Phenylpropanal also observed.

In the case of **1**, reactions with silver salts (e.g., $AgBF_4$) were complete within seconds, as noted by the rapid precipitation of AgCl, formation of a black precipitate (presumably Pd black), full consumption of the starting material, and quantitative conversion to styrene (^1H NMR). Reactions with $NaBAr^F$ were slower, taking minutes to hours for full consumption of **1**

https://dx.doi.org/10.1021/acs.organomet.0c00584
Organometallics XXXX, XXX, XXX−XXX

depending on the conditions, and were amenable to kinetic analysis (*vide infra*). Reactions with zinc salts also afforded styrene, albeit typically at rates slower than the reactions with silver reagents and not always as cleanly. Thus, treatment of **1** in acetonitrile with $ZnCl_2$ led to quantitative styrene formation within seconds, even when the reaction was performed with substoichiometric amounts (33%), but $Zn(OAc)_2$ and ZnO produced styrene in only 77% and 24% yields, respectively, after 22 h.

Monitoring of reactions of **1** and $NaBAr^F$ by ^1H NMR spectroscopy revealed the disappearance of the peaks associated with **1** concomitant with formation of styrene and growth of a doublet attributed to the phosphonium $HP^tBu_3^+$ (Figure S4). No other species were observed, implying that halide abstraction is rate-determining and all subsequent steps are facile (deinsertion, β-hydride elimination). Consistent with this conclusion and a first-order dependence on **1**, a plot of ln[**1**] vs time where $[NaBAr^F]_0 = 5.6 \times 10^{-2}$ M and $[\mathbf{1}]_0 = 1.3 \times 10^{-2}$ M is linear (Chart 1a). Performing the reaction at various concentrations of $NaBAr^F$ (>[**1**]) and plotting versus the observed rate constants also yield a linear fit, consistent with a first-order dependence on $NaBAr^F$ (Chart 1b).[17] Taken together, the data are consistent with rate = $k[\mathbf{1}][NaBAr^F]$, indicative of rate-determining halide abstraction.

Chart 1. (a) Selected Example of a Kinetic Plot for the Reaction between 1 and $NaBAr^F$ in Acetonitrile-d_3[a] and (b) Plot of k_{obs} (Average of Triplicate Measurements; See Figure S5) vs [$NaBAr^F$], Where [Pd-acyl]$_0$ = 0.013 M[b]

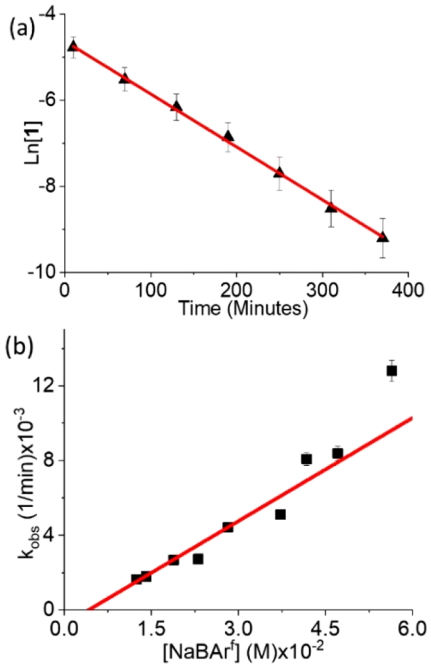

[a] $[\mathbf{1}]_0 = 1.3 \times 10^{-2}$ M, $[NaBAr^F]_0 = 5.6 \times 10^{-2}$ M, $k_{obs} = 3.11 \times 10^{-3}$ min^{-1}, $R^2 = 0.995$. [b] The indicated linear fit has the slope 0.184 M min^{-1} and intercept -7.7×10^{-4} M; $R^2 = 0.953$.

While the results of the reactions of **1** with silver and zinc salts and $NaBAr^F$ suggest that CO deinsertion is activated by the removal of chloride, it is also possible, particularly in the case of the zinc salts, that deinsertion is promoted by binding of the Lewis acid to the carbonyl group. Indeed, 1,3-diisopropyl-2-thiourea, which is known to hydrogen bond with and activate carbonyl compounds,[18] induces consumption of **1** to generate styrene, albeit in a modest 64% yield after 22 h with the formation of side products that could not be easily identified.

In contrast to the reactions of **1**, treatment of **2** with silver and zinc salts and $NaBAr^F$ under the same conditions produced very little styrene (<10%). Instead, a new species was observed by ^1H NMR spectroscopy that we assign as the cationic product of substitution of chloride by CH_3CN, $\mathbf{2}^+$. The species exhibits peaks in the ^1H NMR spectrum similar to those of **2**, except for a slight downfield shift of the methylene protons of the hydrocinnamoyl ligand. We conclusively identified $\mathbf{2}^+$ by isolating it as either its BF_4^- or SbF_6^- salt as a white solid and obtaining the X-ray crystal structure for the latter case (Figure 2).[19] The complex is square planar, with two *trans*-PPh_3 ligands and an acetonitrile molecule replacing the chloride ligand found in **2**; a single SbF_6^- counterion is present (not shown), consistent with a monocationic Pd(II) species.

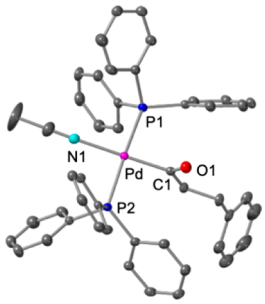

Figure 2. Representation of the X-ray crystal structure of **2**(SbF_6) showing all non-hydrogen atoms as 50% thermal ellipsoids and the SbF_6 counterion omitted for clarity. Selected bond distances (Å): Pd−C(1) 1.9915(19), Pd−N(1) 2.1606(17), Pd−P(1) 2.3513(5), Pd−P(2) 2.3548(5), O(1)−C(1) 1.199(2).

The isolation of $\mathbf{2}^+$ indicates that decarbonylation is significantly slowed relative to **1**. Consistent with this conclusion, while thermolysis of **1** (65 °C, CD_3CN, 12 h) quantitatively afforded styrene, heating **2**(BF_4) under identical conditions produced styrene in only a 37% yield with 16% of **2**(BF_4) remaining. Treatment of **2**(BF_4) with $ZnCl_2$ (1.5 equiv) in CH_2Cl_2/CH_3CN (9/1) produced a small amount of styrene (10% yield). This result is consistent with some decarbonylation promoted by Lewis acid coordination to the carbonyl in the cationic complex. Overall, the sluggish decarbonylation of **2** contrasts with the reactivity observed for **1**, pointing toward significant differences in the accessibility of the necessary transition state geometry imposed by the different phosphine ligands (*vide infra*).

Finally, anticipating that in **3** a *cis* arrangement of the acyl and chloride ligands might lead to enhanced reactivity upon chloride removal, we examined the reactivity of **3** with silver salts. Addition of 1.5 equiv of $AgBF_4$ to a solution of **3** in CD_2Cl_2/CD_3CN (9/1) revealed the formation of styrene (18%), 3-phenylpropanal (33%), and a new species assigned as $\mathbf{4}^+$ (39%; Scheme 3). This assignment was based on ^1H, COSY, $^{13}C\{^1H\}$, and ^{31}P NMR spectroscopy (Figure S9). Attempts to isolate $\mathbf{4}^+$ by filtering the reaction mixture into diethyl ether at −35 °C led to a yellow solid that exhibited the same NMR spectra when it was dissolved in CD_2Cl_2, but when it was dissolved in CD_3CN peaks analogous to those assigned to $\mathbf{2}^+$ were observed, leading to an assignment as $\mathbf{3}^+$ that we

https://dx.doi.org/10.1021/acs.organomet.0c00584
Organometallics XXXX, XXX, XXX−XXX

Scheme 3. Halide Abstraction Reactions of 3[a]

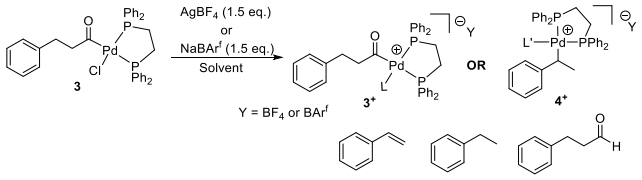

[a]Product mixtures are dependent on the solvent conditions. L is postulated to be acetonitrile, and L′ is postulated to be carbon monoxide or an empty coordination site, blocked by the methyl group of the complex, perhaps stabilized by β-agostic interactions.

surmise is effectively trapped by the solvent prior to decarbonylation. Curious if 4^+ could be an intermediate in styrene production or if longer reaction times would lead to greater yields, we treated **3** with $NaBAr^F$ (1.5 equiv) in CD_2Cl_2/CD_3CN (9/1) (Figure S10). The reaction yielded styrene (14%), aldehyde (30%), ethylbenzene (6%), and 4^+ (46%), with the concentration of styrene and aldehyde products remaining constant after 12 h as 4^+ gradually decayed to more ethylbenzene and there was no further increase in styrene concentration. From these results we conclude that **3** is more prone to decarbonylation than **2** but that the subsequent reactions of the initial Pd-ethylbenzene complex are complicated by reversible chain walking and the possible intermediacy of a hydride species that would be responsible for aldehyde and ethylbenzene formation.[20] The observed increased tendency for decarbonylation is consistent with reports of bidentate ligands facilitating decarbonylation in decarbonylative cross couplings, whereas monodentate ligands typically do not.[21]

Theory. In order to gain insight into the reactivity differences observed experimentally, the structures of **1**−**3** and their dehydrogenative decarbonylation reactions were explored by DFT calculations (computational details are given in the Supporting Information). We first examined the decarbonylation pathways via thermolysis. The CO deinsertion step for **1** proceeds *via* a transition state with a free energy barrier of 22.8 kcal/mol (Figure 3). The equivalent barriers for **2** and **3** are 33.1 and 28.9 kcal/mol, respectively. The lower barrier calculated for **1** is consistent with the experimental observation that upon heating **1** is most effective at producing styrene, albeit slowly.

Next, the decarbonylation process was studied including prior halide abstraction. The data reported in the energy profile (Figure 3) involve Ag^+ ions as the halide-abstracting agent (these results are compared to those obtained using Na^+ ions in Figure S11). If chloride is abstracted using Ag^+ followed by explicit solvation of the Pd center by acetonitrile ($\Delta G = -1.0$ kcal/mol), the free energy barrier for the CO deinsertion step for **1** is lowered by 8.0 kcal/mol to $\Delta G^{\ddagger} = 14.8$ kcal/mol (Figure 3). If the CH_3CN molecule is not explicitly coordinated to Pd, the energy barrier is higher ($\Delta G^{\ddagger} = 16.5$ kcal/mol).

Both **2** ($L_n = PPh_3$) and **3** (L_n = dppe) undergo CO deinsertion reactions similar to that of **1** ($L_n = P^tBu_3$; Figure 3). A similar amount of free energy is required in the bond-making and -breaking processes in the transition state structures for all three ligands ($\Delta G^{\ddagger}$ = 12.1, 11.3, and 11.0 kcal/mol, respectively). However, coordination by acetonitrile after chloride abstraction in **1** produces a slightly unstable intermediate, which subsequently undergoes CO deinsertion. Explicit solvation facilitates the reaction by allowing the transition state structure to maintain a stable four-coordinate

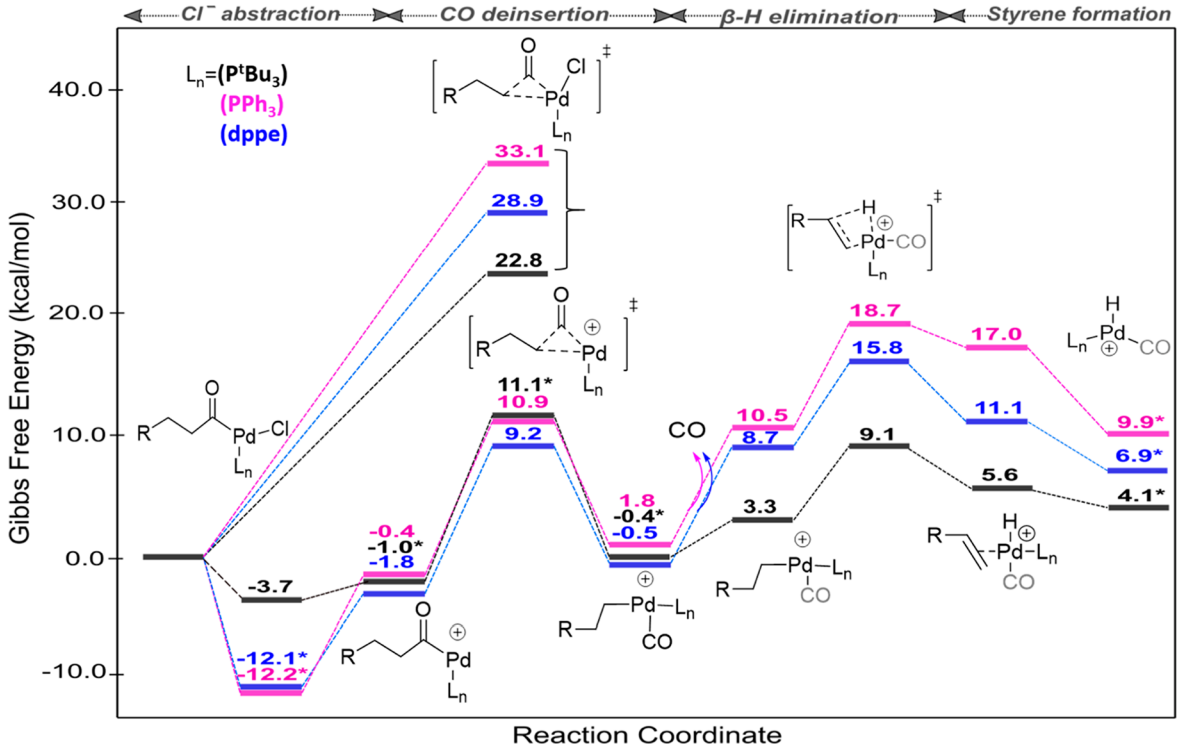

Figure 3. DFT computed reaction mechanism for Pd-catalyzed decarbonylation of 3-Phenylpropionyl chloride. Asterisks indicate the coordination of an explicit acetonitrile (solvent) molecule. When CO is shown in gray, it is only coordinated in the black (P^tBu_3) pathway.

https://dx.doi.org/10.1021/acs.organomet.0c00584
Organometallics XXXX, XXX, XXX−XXX

geometry at the Pd(II) center (Figure 4). On the other hand, in complexes **2** and **3**, the most favorable transition state

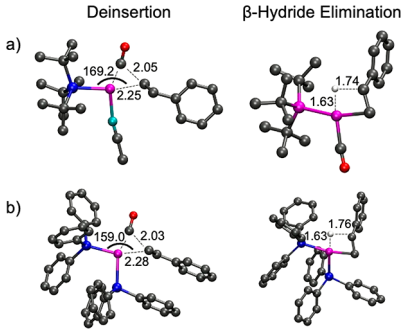

Figure 4. Deinsertion and β-hydride elimination optimized transition state geometries for the pathways with the (a) P^tBu_3 and (b) PPh_3 ligands. Bond distances are given in Å and angles in degrees. Hydrogen atoms not involved in β-hydride elimination are excluded for clarity. Color code: P, blue; Pd, magenta; C, gray; O, red; N, teal.

structures are not solvated, since they are already four-coordinate. The stability of the cationic intermediates $\mathbf{2}^+$ (ΔG = −12.2 kcal/mol) and $\mathbf{3}^+$ (ΔG = −12.1 kcal/mol) leads to higher barriers for CO deinsertion of 23.1 and 21.3 kcal/mol, respectively. Thus, while for **1** CO deinsertion is significantly hastened after halide abstraction relative to direct thermolysis, for both **2** and **3** the two routes have similarly high barriers.

Further insight into the CO deinsertion process comes from an analysis of the calculated transition state geometries. The respective transition states have P−Pd−C angles ranging from 169.2° with P^tBu_3 to 159.0° with PPh_3 (Figure 4 and Figure S12). The structure with P^tBu_3 has the shortest distance for the newly formed Pd−C bond (2.25 Å), signifying stronger bonds that stabilize the transition state structure. For the dppe transition state (Figure S12), the P−Pd−C angle is 167.6° and the Pd−C bond distance is 2.28 Å. We surmise that the presence of a single P^tBu_3 ligand results in more favorable CO deinsertion because of a relative lack of destabilizing steric effects. Also, in the CO deinsertion for the case of PPh_3, the *trans* phosphine ligands must rotate to the *cis* position in the transition state, and this requires 4.2 kcal/mol. We speculate that steric effects associated with the *cis* arrangement further add to the energetic cost for CO deinsertion in this case (Scheme S8). For the case of the bidentate dppe ligand, the *trans* arrangement is inaccessible, and the transition state exhibits steric characteristics that fall between those of P^tBu_3 and PPh_3. The CO deinsertion products are ∼10 kcal/mol lower in energy than the TS barriers.

The findings from the above analysis are in agreement with the results of other studies.[13] For example, it was observed that PPh_3 ligands decoordinate from a Pd catalyst during the decarbonylative dehydration of butanoic acid to maintain four-coordinate complexes, while the ligand remains coordinated to the less active Rh analogue.[13b] Also, in an analysis of the turnover-limiting step in the formation of styrene from hydrocinnamic acid by a Pd catalyst with a PPh_3 ligand, it was observed that the four-coordinate transition state structures are more stable than the five-coordinate structures.[13a] Furthermore, the use of a bulkier phosphine was predicted to lower the barrier by ∼10 kcal/mol.

Turning next to the β-hydride elimination step, we find that the transition state with P^tBu_3 has the lowest energy barrier (9.5 kcal/mol) in comparison to the values of 16.9 and 16.3 kcal/mol for the cases with PPh_3 and dppe, respectively (Figure 3 and Schemes S13 and S14). This calculated trend aligns with that seen by experiment, insofar as reactions beginning with **1** produce styrene rapidly and quantitatively, while **2** and **3** produce smaller yields of styrene. Although solvation stabilizes CO deinsertion when P^tBu_3 is used, β-hydride elimination is more favorable without explicit solvation, which allows for a planar, four-coordinate geometry to be maintained in the transition state wherein P^tBu_3 and CO occupy *cis* positions. Despite the analogous PPh_3 and dppe TS structures having two phosphine groups coordinating to the metal, the most favorable pathways also maintain a four-coordinate Pd center since CO is decoordinated prior to β-hydride elimination.

Overall, the calculations show that β-hydride elimination is the rate-determining transition state (RDTS), defined by the highest energy transition state, for PPh3 and dppe. Additionally, the presence of the stable halide elimination product for **2** and **3** significantly increases the energy required to form styrene and is not captured by the RDTS alone. The barriers from this determining intermediate to the highest transition state are 14.8, 30.9, and 27.9 kcal/mol for **1**−**3**, respectively.

CONCLUSION

The dehydrative decarbonylation of $(L_n)Pd^{II}(Cl)$-hydrocinnamoyl complexes (L = P^tBu_3, n = 1; L = PPh_3, n = 2; L = dppe, n = 1) was evaluated through experiment and theory with the primary aim of understanding how changes in the nature of the supporting phosphine ligand(s) influences the efficiency of styrene formation and the energetics of the proposed reaction steps. Removal of the chloride ligand was found to enhance the production of styrene, with the complex of P^tBu_3 being the most efficient. A solvento intermediate resulting from chloride abstraction was structurally characterized for the complex of PPh_3, and a related species was implicated on the basis of NMR spectroscopy for the complex of dppe. DFT calculations revealed β-hydride elimination from a stable intermediate formed upon halide abstraction to be rate-determining for the overall dehydrative decarbonylation. The barrier heights for this step and the CO deinsertion step followed the trend P^tBu_3 < dppe < PPh_3, consistent with the experimentally observed dependence of styrene production efficiency on the supporting ligand (P^tBu_3 > dppe > PPh_3). A key overall conclusion is that coordinative desaturation through chloride removal and use of the highly sterically hindered P^tBu_3 greatly facilitate dehydrative decarbonylation. In addition, the enforcement of a *cis* disposition of phosphine donors in dppe is beneficial relative to the complex comprising PPh_3 ligands. We hope that these notions determined through a study of a particular Pd-based test system will inform future efforts to design new catalysts for the generation of olefins from bioderived carboxylic acids.

ASSOCIATED CONTENT

Supporting Information

The Supporting Information is available free of charge at https://pubs.acs.org/doi/10.1021/acs.organomet.0c00584.

Cartesian coordinates (XYZ)

Experimental and computational details and spectra (PDF)

https://dx.doi.org/10.1021/acs.organomet.0c00584
Organometallics XXXX, XXX, XXX−XXX

Accession Codes

CCDC 2023533−2023535 contain the supplementary crystallographic data for this paper. These data can be obtained free of charge via www.ccdc.cam.ac.uk/data_request/cif, or by emailing data_request@ccdc.cam.ac.uk, or by contacting The Cambridge Crystallographic Data Centre, 12 Union Road, Cambridge CB2 1EZ, UK; fax: +44 1223 336033.

AUTHOR INFORMATION

Corresponding Authors

Bess Vlaisavljevich − *University of South Dakota, Vermillion, South Dakota 57069, United States;* orcid.org/0000-0001-6065-0732; Email: bess.vlaisavljevich@usd.edu

William B. Tolman − *Department of Chemistry and Center for Sustainable Polymers, Washington University in St. Louis, St. Louis, Missouri 63130-4899, United States;* orcid.org/0000-0002-2243-6409; Email: wbtolman@wustl.edu

Authors

Tedd C. Wiessner − *Department of Chemistry and Center for Sustainable Polymers, Washington University in St. Louis, St. Louis, Missouri 63130-4899, United States;* orcid.org/0000-0002-5221-7389

Samuel Asiedu Fosu − *University of South Dakota, Vermillion, South Dakota 57069, United States;* orcid.org/0000-0002-7816-094X

Riffat Parveen − *University of South Dakota, Vermillion, South Dakota 57069, United States;* orcid.org/0000-0003-4941-7512

Nigam P. Rath − *Department of Chemistry and Biochemistry and Center for Nanoscience, University of Missouri−St. Louis, St. Louis, Missouri 63121, United States*

Complete contact information is available at: https://pubs.acs.org/10.1021/acs.organomet.0c00584

Funding

This work was supported by the NSF Center for Sustainable Polymers, a NSF Center for Chemical Innovation (CHE-1901635). X-ray diffraction data were collected using diffractometers acquired through NSF-MRI Award No. CHE-1827756. Computations were performed on high performance computing systems at the University of South Dakota, funded by NSF Award No. CHE-1626516. Mass spectrometry data were collected at the Washington University NIGMS Biomedical Mass Spectrometry Resource supported by NIH grants 5P41GM103422 and R24GM136766.

Notes

The authors declare no competing financial interest.

ACKNOWLEDGMENTS

We thank Jong Hee Song for the acquisition and analysis of mass spectrometry data. All primary data files are available free of charge at 10.13020/xpa3-w249.

REFERENCES

(1) Keim, W. Oligomerization of Ethylene to α-Olefins: Discovery and Development of the Shell Higher Olefin Process (SHOP). *Angew. Chem., Int. Ed.* **2013**, *52*, 12492−12496.

(2) Zhang, X.; Jordan, F.; Szostak, M. Transition-Metal-Catalyzed Decarbonylation of Carboxylic Acids to Olefins: Exploiting Acyl C-O Activation for the Production of High Value Products. *Org. Chem. Front.* **2018**, *5*, 2515−2521.

(3) Chatterjee, A.; Hopen Eliasson, S. H.; Jensen, V. R. Selective Production of Linear α-Olefins: Via Catalytic Deoxygenation of Fatty Acids and Derivatives. *Catal. Sci. Technol.* **2018**, *8* (6), 1487−1499.

(4) (a) John, A.; Dereli, B.; Ortunío, M. A.; Johnson, H. E.; Hillmyer, M. A.; Cramer, C. J.; Tolman, W. B. Selective Decarbonylation of Fatty Acid Esters to Linear α-Olefins. *Organometallics* **2017**, *36*, 2956−2964. (b) John, A.; Hogan, L. T.; Hillmyer, M. A.; Tolman, W. B. Olefins from Biomass Feedstocks: Catalytic Ester Decarbonylation and Tandem Heck-Type Coupling. *Chem. Commun.* **2015**, *51*, 2731−2733.

(5) (a) Miranda, M. O.; Pietrangelo, A.; Hillmyer, M. A.; Tolman, W. B. Catalytic Decarbonylation of Biomass-Derived Carboxylic Acids as Efficient Route to Commodity Monomers. *Green Chem.* **2012**, *14*, 490−494. (b) John, A.; Miranda, M. O.; Ding, K.; Dereli, B.; Ortuno, M. A.; Lapointe, A. M.; Coates, G. W.; Cramer, C. J.; Tolman, W. B. Nickel Catalysts for the Dehydrative Decarbonylation of Carboxylic Acids to Alkenes. *Organometallics* **2016**, *35*, 2391−2400. (c) Le Notre, J.; Scott, E. L.; Franssen, M. C.R.; Sanders, J. P.M. Selective Preparation of Terminal Alkenes from Aliphatic Carboxylic Acids by a Palladium-Catalysed Decarbonylation-Elimination Reaction. *Tetrahedron Lett.* **2010**, *51*, 3712−3715. (d) Miller, J. A.; Nelson, J. A.; Byrne, M. P. A Highly Catalytic and Selective Conversion of Carboxylic Acids to 1-Alkenes of One Less Carbon Atom. *J. Org. Chem.* **1993**, *58*, 18−20.

(6) Tsuji, J.; Ohno, K. Organic Syntheses by Means of Noble Metal Compounds. XXXIV. Carbonylation and Decarbonylation Reactions Catalyzed by Palladium. *J. Am. Chem. Soc.* **1968**, *90*, 94−98.

(7) Foglia, T. A.; Barr, P. A. Decarbonylation Dehydration of Fatty Acids to Alkenes in the Presence of Transition Metal Complexes. *J. Am. Oil Chem. Soc.* **1976**, *53*, 737−741.

(8) (a) Murray, R. E.; Walter, E. L.; Doll, K. M. Tandem Isomerization-Decarboxylation for Converting Alkenoic Fatty Acids into Alkenes. *ACS Catal.* **2014**, *4*, 3517−3520. (b) Fieser, M. E.; Schimler, S. D.; Mitchell, L. A.; Wilborn, E. G.; John, A.; Hogan, L. T.; Benson, B.; LaPointe, A. M.; Tolman, W. B. Dual-Catalytic Decarbonylation of Fatty Acid Methyl Esters to Form Olefins. *Chem. Commun.* **2018**, *54*, 7669−7672.

(9) (a) Ternel, J.; Lebarbé, T.; Monflier, E.; Hapiot, F. Catalytic Decarbonylation of Biosourced Substrates. *ChemSusChem* **2015**, *8*, 1585−1592. (b) Maetani, S.; Fukuyama, T.; Suzuki, N.; Ishihara, D.; Ryu, I. Efficient Iridium-Catalyzed Decarbonylation Reaction of Aliphatic Carboxylic Acids Leading to Internal or Terminal Alkenes. *Organometallics* **2011**, *30*, 1389−1394.

(10) Maetani, S.; Fukuyama, T.; Suzuki, N.; Ishihara, D.; Ryu, I. Iron-Catalyzed Decarbonylation Reaction of Aliphatic Carboxylic Acids Leading to α-Olefins. *Chem. Commun.* **2012**, *48*, 2552−2554.

(11) (a) Gooßen, L. J.; Rodríguez, N. A Mild and Efficient Protocol for the Conversion of Carboxylic Acids to Olefins by a Catalytic Decarbonylative Elimination Reaction. *Chem. Commun.* **2004**, *4*, 724−725. (b) Liu, Y.; Kim, K. E.; Herbert, M. B.; Fedorov, A.; Grubbs, R. H.; Stoltz, B. M. Palladium-Catalyzed Decarbonylative Dehydration of Fatty Acids for the Production of Linear Alpha Olefins. *Adv. Synth. Catal.* **2014**, *356*, 130−136. (c) Chatterjee, A.; Hopen Eliasson, S. H.; Törnroos, K. W.; Jensen, V. R. Palladium Precatalysts for Decarbonylative Dehydration of Fatty Acids to Linear Alpha Olefins. *ACS Catal.* **2016**, *6*, 7784−7789.

(12) (a) Cheng, W.-M.; Shang, R.; Fu, Y. Irradiation-Induced Palladium-Catalyzed Decarboxylative Desaturation Enabled by a Dual Ligand System. *Nat. Commun.* **2018**, *9*, 5215. (b) Tlahuext-Aca, A.; Candish, L.; Garza-Sanchez, R. A.; Glorius, F. Decarboxylative Olefination of Activated Aliphatic Acids Enabled by Dual Organophotoredox/Copper Catalysis. *ACS Catal.* **2018**, *8*, 1715−1719. (c) Sun, X.; Chen, J.; Ritter, T. Catalytic Dehydrogenative Decarboxyolefination of Carboxylic Acids. *Nat. Chem.* **2018**, *10*, 1229−1233. (d) Nguyen, V. T.; Nguyen, V. D.; Haug, G. C.; Dang, H. T.; Jin, S.; Li, Z.; Flores-Hansen, C.; Benavides, B. S.; Arman, H. D.; Larionov, O. V. Alkene Synthesis by Photocatalytic Chemoenzymatically Compatible Dehydrodecarboxylation of Carboxylic Acids and Biomass. *ACS Catal.* **2019**, *9*, 9485−9498.

(13) (a) Ortuño, M. A.; Dereli, B.; Cramer, C. J. Mechanism of Pd-Catalyzed Decarbonylation of Biomass-Derived Hydrocinnamic Acid to Styrene Following Activation as an Anhydride. *Inorg. Chem.* **2016**, *55*, 4124−4131. (b) Eliasson, S.; Chatterjee, A.; Occhipinti, G.; Jensen, V. The Mechanism of Rh-Catalyzed Transformation of Fatty Acids to Linear Alpha Olefins. *Inorganics* **2017**, *5*, 87.

(14) (a) Gao, B.; Zhang, G.; Zhou, X.; Huang, H. Palladium-Catalyzed Regiodivergent Hydroaminocarbonylation of Alkenes to Primary Amides with Ammonium Chloride. *Chem. Sci.* **2018**, *9*, 380−386. (b) Clavier, H.; Nolan, S. P. Percent Buried Volume for Phosphine and N-Heterocyclic Carbene Ligands: Steric Properties in Organometallic Chemistry. *Chem. Commun.* **2010**, *46*, 841−861. (c) Bilbrey, J. A.; Kazez, A. H.; Locklin, J.; Allen, W. D. Exact Ligand Cone Angles. *J. Comput. Chem.* **2013**, *34*, 1189−1197.

(15) (a) Quesnel, J. S.; Kayser, L. V.; Fabrikant, A.; Arndtsen, B. A. Acid Chloride Synthesis by the Palladium-Catalyzed Chlorocarbonylation of Aryl Bromides. *Chem. - Eur. J.* **2015**, *21*, 9550−9555. (b) Campos, J.; Nova, A.; Kolychev, E. L.; Aldridge, S. A Combined Experimental/Computational Study of the Mechanism of a Palladium-Catalyzed Bora-Negishi Reaction. *Chem. - Eur. J.* **2017**, *23*, 12655−12667.

(16) Lin, Y. S.; Yamamoto, A. Studies Relevant to Palladium-Catalyzed Carbonylation Processes. Mechanisms of Formation of Esters and Amides from Benzylpalladium and (Phenylacetyl) Palladium Complexes on Reactions with Alcohols and Amines. *Organometallics* **1998**, *17*, 3466−3478.

(17) The value for the k_{obs} value at the highest [$NaBAr^F_4$] appears to be anomalously high, the reason(s) for which is (are) unclear.

(18) (a) Nickerson, D. M.; Angeles, V. V.; Auvil, T. J.; So, S. S.; Mattson, A. E. Internal Lewis Acid Assisted Ureas: Tunable Hydrogen Bond Donor Catalysts. *Chem. Commun.* **2013**, *49*, 4289−4291. (b) Lu, A.; Wang, Z.; Zhou, Z.; Chen, J.; Wang, Q. Application of "Hydrogen Bonding Interaction" in New Drug Development: Design, Synthesis, Antiviral Activity, and Sars of Thiourea Derivatives. *J. Agric. Food Chem.* **2015**, *63* (5), 1378−1384.

(19) Analogous species have been reported previously: (a) Brumbaugh, J. S.; Sen, A. Mechanism of Acyl Group Isomerization in Palladium(II) Complexes. Development of a Catalytic Process for the Isomerization of Carboxylic Acid Chlorides. *J. Am. Chem. Soc.* **1988**, *110*, 803−816. (b) Lagueux-Tremblay, P.-L.; Fabrikant, A.; Arndtsen, B. A. Palladium-Catalyzed Carbonylation of Aryl Chlorides to Electrophilic Aroyl-DMAP Salts,. *ACS Catal.* **2018**, *8*, 5350−5354.

(20) We further note that omitting acetonitrile or replacing it with noncoordinating nitromethane leads to the sole formation of $\mathbf{4}^+$, whereas reactions in pure acetonitrile lead to only styrene, 3-phenylpropanal, and unidentified decomposition products. Out of curiosity, we subjected **2** to halide abstraction conditions without acetonitrile and observed a species we tentatively assign as the PPh_3-coordinated analogue of $\mathbf{4}^+$ (for discussion/characterization on these Pd-2-ethylbenzene complexes see the Supporting Information and Figures S6 and S7). As in the case of **2**, the reaction of **3** with $ZnCl_2$ showed the largest amount of styrene (45%), also producing aldehyde (52%) and $\mathbf{4}^+$ (18%). The reaction of $Zn(OAc)_2$ led to styrene and 2-phenylpropanal in 24 and 32% yields, respectively, but no $\mathbf{4}^+$, while ZnO and diisopropylthiourea showed no reactivity.

(21) (a) Masson-Makdissi, J.; Vandavasi, J. K.; Newman, S. G. Switchable Selectivity in the Pd-Catalyzed Alkylative Cross-Coupling of Esters. *Org. Lett.* **2018**, *20*, 4094−4098. (b) Ogiwara, Y.; Sakurai, Y.; Hattori, H.; Sakai, N. Palladium-Catalyzed Reductive Conversion of Acyl Fluorides via Ligand-Controlled Decarbonylation. *Org. Lett.* **2018**, *20*, 4204−4208. (c) Hong, X.; Liang, Y.; Houk, K. N. Mechanisms and Origins of Switchable Chemoselectivity of Ni-Catalyzed C(Aryl)-O and C(Acyl)-O Activation of Aryl Esters with Phosphine Ligands. *J. Am. Chem. Soc.* **2014**, *136*, 2017−2025. (d) Chatupheeraphat, A.; Liao, H. H.; Srimontree, W.; Guo, L.; Minenkov, Y.; Poater, A.; Cavallo, L.; Rueping, M. Ligand-Controlled Chemoselective C(Acyl)-O Bond vs C(Aryl)-C Bond Activation of Aromatic Esters in Nickel Catalyzed C(Sp2)-C(Sp3) Cross-Couplings. *J. Am. Chem. Soc.* **2018**, *140*, 3724−3735. (e) Liu, C.; Ji, C. L.; Qin, Z. X.; Hong, X.; Szostak, M. Synthesis of Biaryls via Decarbonylative Palladium-Catalyzed Suzuki-Miyaura Cross-Coupling of Carboxylic Acids. *iScience* **2019**, *19*, 749−759.

https://dx.doi.org/10.1021/acs.organomet.0c00584
Organometallics XXXX, XXX, XXX−XXX